ESC European Society of Cardiology

Cardiovascular Research (2023) **119**, 1568–1582
https://doi.org/10.1093/cvr/cvad037

Phospholamban pentamerization increases sensitivity and dynamic range of cardiac relaxation

Florian Funk[1], Annette Kronenbitter[1], Katarzyna Hackert[1], Matthias Oebbeke[2], Gerhard Klebe[2], Mareike Barth[3], Daniel Koch[4], and Joachim P. Schmitt [1]*

[1]Institute of Pharmacology, University Hospital Düsseldorf, and Cardiovascular Research Institute Düsseldorf (CARID), Heinrich-Heine-University, Universitätsstraße 1, 40225 Düsseldorf, Germany; [2]Institute of Pharmaceutical Chemistry, Philipps-University Marburg, Marbacher Weg 6, 35032 Marburg, Germany; [3]Department of Cardiovascular Surgery, University Hospital Düsseldorf, Heinrich-Heine-University, Moorenstr. 5, 40225 Düsseldorf, Germany; and [4]Max Planck Institute for Neurobiology of Behavior—caesar, Cellular computations and learning group, Ludwig-Erhard-Allee 2, 53175 Bonn, Germany

Received 8 June 2022; revised 4 November 2022; accepted 20 December 2022; online publish-ahead-of-print 3 March 2023

Time of primary review: 29 days

Aims

A key event in the regulation of cardiac contraction and relaxation is the phosphorylation of phospholamban (PLN) that relieves the inhibition of the sarco/endoplasmic reticulum (SR) Ca^{2+}-ATPase (SERCA2a). PLN exists in an equilibrium between monomers and pentamers. While only monomers can inhibit SERCA2a by direct interaction, the functional role of pentamers is still unclear. This study investigates the functional consequences of PLN pentamerization.

Methods and results

We generated transgenic mouse models expressing either a PLN mutant that cannot form pentamers (TgAFA-PLN) or wild-type PLN (TgPLN) in a PLN-deficient background. TgAFA-PLN hearts demonstrated three-fold stronger phosphorylation of monomeric PLN, accelerated Ca^{2+} cycling of cardiomyocytes, and enhanced contraction and relaxation of sarcomeres and whole hearts *in vivo*. All of these effects were observed under baseline conditions and abrogated upon inhibition of protein kinase A (PKA). Mechanistically, far western kinase assays revealed that PLN pentamers are phosphorylated by PKA directly and independent of any subunit exchange for free monomers. *In vitro* phosphorylation of synthetic PLN demonstrated that pentamers even provide a preferred PKA substrate and compete with monomers for the kinase, thereby reducing monomer phosphorylation and maximizing SERCA2a inhibition. However, β-adrenergic stimulation induced strong PLN monomer phosphorylation in TgPLN hearts and sharp acceleration of cardiomyocyte Ca^{2+} cycling and haemodynamic values that now were indistinguishable from TgAFA-PLN and PLN-KO hearts. The pathophysiological relevance of PLN pentamerization was evaluated using transverse aortic constriction (TAC) to induce left ventricular pressure overload. Compared to TgPLN, TgAFA-PLN mice demonstrated reduced survival after TAC, impaired cardiac haemodynamics, failure to respond to adrenergic stimulation, higher heart weight, and increased myocardial fibrosis.

Conclusions

The findings show that PLN pentamerization greatly impacts on SERCA2a activity as it mediates the full range of PLN effects from maximum inhibition to full release of SERCA2a function. This regulation is important for myocardial adaptation to sustained pressure overload.

* Corresponding author. Tel: +49 211 8112449; fax: +49 211 8114781, E-mail: joachim.schmitt@uni-duesseldorf.de

Graphical Abstract

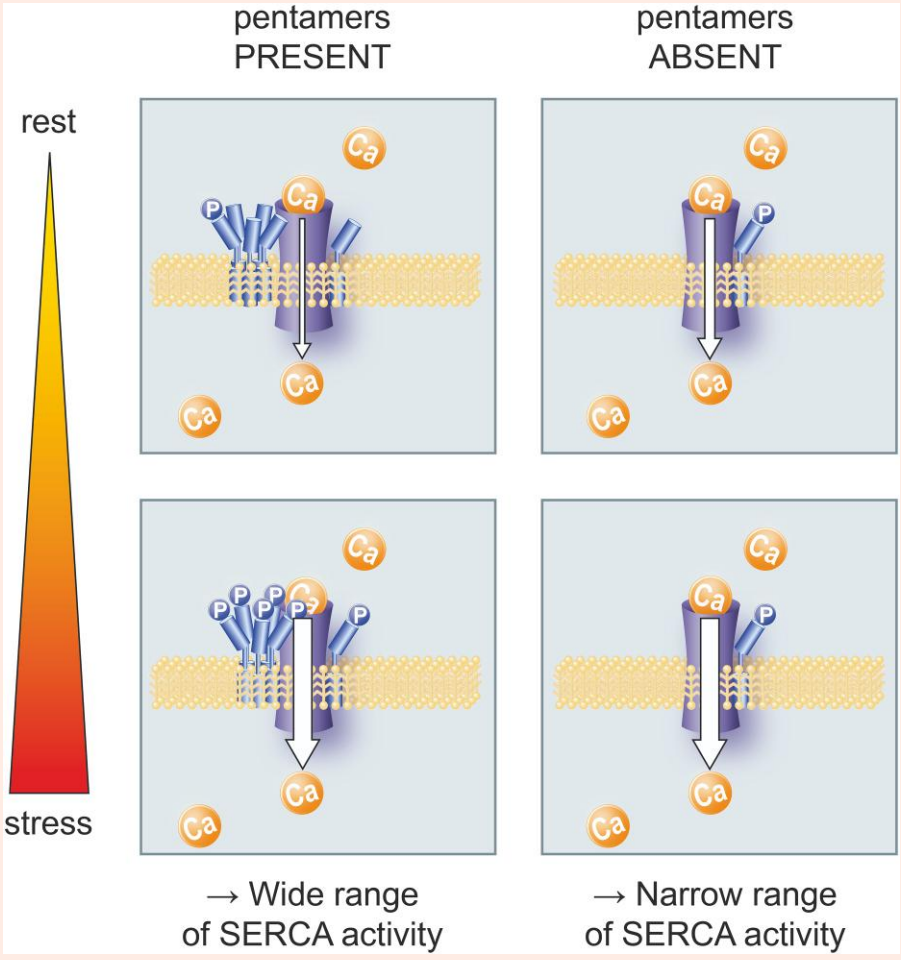

Keywords SERCA2a/phospholamban complex • Cardiomyocyte calcium cycling • Protein kinase A • Sarcomere function • Ventricular pressure overload

1. Introduction

Cardiomyocyte relaxation is initiated by the removal of Ca^{2+} from the cytosol. In ventricular cardiomyocytes, the sarco/endoplasmic reticulum (SR) Ca^{2+}-ATPase (SERCA2a) accounts for a species-dependent 70–95% removal of cytosolic Ca^{2+}.[1] Enhanced SERCA2a activity also increases the amplitude of the systolic Ca^{2+} transient and thereby cardiac contractility.

SERCA2a activity is regulated by stimulatory and inhibitory interactions with regulatory proteins among which phospholamban (PLN) is recognized as the principal SERCA2a regulator. PLN is a 52-residue helical protein that co-localizes with the Ca^{2+}-ATPase in the SR membrane and reduces the Ca^{2+} affinity of SERCA2a by direct interaction. This inhibition is relieved upon protein kinase A (PKA)-dependent phosphorylation of PLN at S16, as upon stimulation of the sympathetic nervous system. To a lesser extent, T17 phosphorylation adds to this regulation.[2]

In lipid bilayers, PLN oligomerizes and monomers co-exist in equilibrium with PLN pentamers that are stabilized by leucine/isoleucine zippers.[3,4] The functional role of PLN pentamers in myocyte Ca^{2+} handling and thus cardiac function—if there is any—is still unclear. A plethora of studies on PLN mutants with different oligomeric ratios provided strong evidence that only PLN monomers inhibit SERCA2a by direct interaction.[5–8] SERCA2a activity hinges on the phosphorylation state of PLN monomers that tend to oligomerize upon phosphorylation.[3,9] The prevailing model thus assumes that PLN pentamers serve as an inactive, non-inhibitory storage form and reservoir for phosphorylated PLN monomers.

However, some studies suggested an active role of PLN pentamers in the regulation of SERCA2a activity. First, crystallographic analyses revealed that PLN pentamers directly interact with SERCA2a at transmembrane segment M3 of the enzyme.[10,11] This association may have functional consequences on the Ca^{2+}-ATPase because proteoliposomes containing SERCA and PLN at different ratios indicated that PLN pentamers increased the maximum rate for Ca^{2+} transport.[12] Further, we and others found evidence that pentamerization can affect PLN phosphorylation, which would alter PLN inhibitory activity.[13–15] Specifically, we found that pentamers delay and reduce PKA-dependent monomer phosphorylation in transfected cell lines and that they enable a bistable system of PLN phosphorylation.

All of these studies have been performed *ex vivo* in non-myocyte cells or *in silico*, but the impact of PLN pentamerization on the phosphorylation patterns in the heart and its (patho–) physiological consequences *in vivo* have not been assessed. The present work investigated the functional effects of PLN pentamerization on cardiomyocyte Ca^{2+} cycling and sarcomere

function in relation to changes of PKA activity using mouse models with and without PLN pentamers. We provide what to our knowledge is the first direct experimental evidence that pentamers are substrates of PKA, thereby impacting on monomer phosphorylation by substrate competition and on the regulation of SERCA2a activity. Pentamers turned out to enhance the sensitivity and dynamic range of Ca^{2+} regulation and myocardial relaxation in response to β-adrenergic stimulation. Thereby, they seemed to facilitate myocardial adaptation to pathological stress, as PLN pentamers improved the structural and functional remodelling of mouse hearts in response to chronic pressure overload.

2. Methods

2.1 Mouse generation, housing

The purely monomeric PLN mutant AFA-PLN was generated by introducing the mutations Cys36Ala, Cys41Phe, and Cys46Ala into PLN mouse cDNA. Wild-type PLN and AFA-PLN were cloned downstream of the mouse α-myosin heavy chain (Myh6) promoter, and the cDNA constructs were injected into pronuclei of fertilized FVB/N oocytes as previously described.[16,17] Founder mice with transgene expression close to physiological levels of PLN expression were crossed with PLN-deficient mice (FVB/N)[18] to achieve transgenic mice with homozygous deletion of the endogenous PLN gene, designated as TgPLN and TgAFA-PLN. Genotypes were assessed by PCR analysis of tail biopsies. We compared mouse hearts with (TgPLN) and without (TgAFA-PLN) PLN pentamers and transgene negative littermates that harboured neither pentamers nor monomers (PLN-KO).

We further generated transgenic mouse lines carrying the FLAG-sequence (DYKDDDDK) at the *N*-terminus of PLN or AFA-PLN, respectively, designated as TgF-PLN and TgF-AFA-PLN. These mouse lines were used for immunofluorescent detection of subcellular transgene location and for detection of PLN and AFA-PLN independent of PLN-specific antibodies during western blot analyses (*Figure 2D*). All mice were housed in a specified pathogen-free facility and maintained on an inbred FVB/N genetic background. Care of the animals was in accordance with the Committee on Animal Research of the responsible authorities (Regierung von Unterfranken and Landesamt für Natur, Umwelt- und Verbraucherschutz Nordrhein-Westfalen, Germany) that reviewed and approved all experimental protocols (Az. 54-2531.01-58/06, Az. 55.2-2531.01-46/09, Az. 54-2531.01-20/10, Az. 84-02.04.2013.A122, and Az.81-02.04.2021.A155). All procedures conformed to the guidelines from Directive 2010/63/EU of the European Parliament on the protection of animals used for scientific purposes. If not noted otherwise, anaesthesia of animals was performed by a single intraperitoneal injection of 100 μg ketamine per gram body weight plus 10 μg xylazine per gram body weight, and intraoperative analgesia was enhanced by subcutaneous injection of 0.05 μg buprenorphine per gram body weight 30 min before the procedure. At the end of the study, all mice were euthanized by quick manual cervical dislocation.

2.2 Transverse aortic constriction, TAC

Transverse aortic constriction (TAC) to induce left ventricular pressure overload was performed as previously described.[19,20] In brief, the aorta between the innominate artery and the left common carotid artery of anaesthetized and ventilated mice at the age of 8 weeks was exposed by partial thoracotomy and ligated against a 27-gauge needle using a 7–0 silk thread. The needle was quickly removed to leave a discrete stenosis before chest closure and extubation of mice. Sham-operated animals underwent the same procedure except for the ligation of the aorta.

2.3 Echocardiography

Transthoracic echocardiograms were obtained using a Vevo2100 high-resolution imaging systems (VisualSonics) and a 30-MHz probe. Mice were anesthetized with pentobarbital (30 μg/g body weight i.p.), positioned on a heating pad to maintain body temperature and attached to an electrocardiogram monitor. End-diastolic anterior and posterior wall thicknesses as well as end-diastolic and end-systolic diameters were measured in M-mode images of midventricular long and short axis views. Peak blood flow velocities were obtained at the site of TAC by pulsed-wave Doppler measurements. Cardiac Measurements software (VisualSonics) was used for calculation of left ventricular fractional shortening, end-diastolic and end-systolic volumes and aortic pressure gradients. All data were acquired and analysed by a single investigator, who was blinded for the mouse genotype during measurements and data analysis. Measurements were performed at physiological heart rates (>430 beats per minute).

2.4 Measurements of haemodynamics

Left ventricular pressures, rates of pressure rise (dp/dt_{max}), rates of pressure decay (dp/dt_{min}), and heart rates were obtained as previously described.[21] A 1.4 F pressure catheter (Millar Instruments) was inserted into the left ventricle via the right carotid artery of anesthetized 8-week-old study mice, and dobutamine was infused via the left jugular vein at increasing rates (75, 150, 375, 750, and 1500 ng/min) during the recordings. Owing to the deep anaesthesia during the invasive procedure, basal heart rates were lower than during echocardiography; animals with basal heart rates below 400 beats per minute were excluded. Data were analysed using Chart software (Chart 5.4, AD Instruments). The investigators were blinded for the genotype of animals during catheterization and data analysis.

2.5 Measurements of Ca^{2+} kinetics and sarcomere mechanics

Hearts of 8 to 10-week-old mice were digested with collagenase type I (Worthington Biochemical Corp., Lakewood, NJ, USA) by retrograde perfusion to isolate ventricular myocytes as described previously.[22] Quality of myocyte isolation was acceptable if morphology of >70% of myocytes was preserved and if 50% of those were contracting upon electrical stimulation with 10 V. Phosphorylation patterns of isolated cardiomyocytes and whole hearts were similar indicating that phosphorylation patterns were preserved during the process of myocyte isolation (see Supplementary material online, *Figure S7C*). Isolated cells were loaded with Ca^{2+} and the fluorescent Ca^{2+} indicator Fura-2 AM (1 μM; Invitrogen) for 15 min, superfused with prewarmed buffer (137 mM NaCl, 5.4 mM KCl, 1.2 mM $CaCl_2$, 1 mM $MgCl_2$, 10 mM HEPES, and 5.5 mM glucose; pH 7.4; 37°C), and paced at 0.5 Hz for assessment of Ca^{2+} transients using a dual-excitation (340 and 380 nm) single-emission (480–520 nm) system (HyperSwitch Myocyte System, IonOptix). A video-based sarcomere length detection system was used for measurements of sarcomere contraction and relaxation (MyoCamS, IonOptix). For blockage of PKA-dependent phosphorylation, myocytes were incubated with the PKA inhibitor H-89 (10^{-5} M) for 15 min at 37°C before the measurements. For β-adrenergic receptor stimulation of cells, 10^{-7} M isoproterenol was added to the perfusion buffer. Data from at least seven cells per heart and at least eight hearts per genotype were analysed in a blinded fashion using IonWizard software (Version 6.4, Milton, MA, USA).

2.6 Histology

For histology, mouse hearts were fixed in 4% paraformaldehyde and embedded in paraffin. Ventricular sections were stained with hematoxylin and eosin or with Sirius Red as described previously.[21] For assessment of fibrosis, the relative proportion of red staining was determined in whole transverse sections derived from transverse sections of left ventricles >100 μm apart from each other and stained in parallel with Sirius Red. Perivascular collagen was excluded from the analyses, and quantification of red stained fibres was performed in a blinded manner using AxioVision SE64 (Release 4.9) and ImageJ software.

2.7 PLN phosphorylation at baseline and upon β-adrenergic receptor stimulation

Mice were anaesthetized by intraperitoneal injection of pentobarbital (50 μg/g bodyweight) and placed on a heating plate (37°C) for 20 min. Then, the mouse was sacrificed by cervical dislocation, cardiac ventricles were quickly excised, snap-frozen in liquid nitrogen within <60 s after

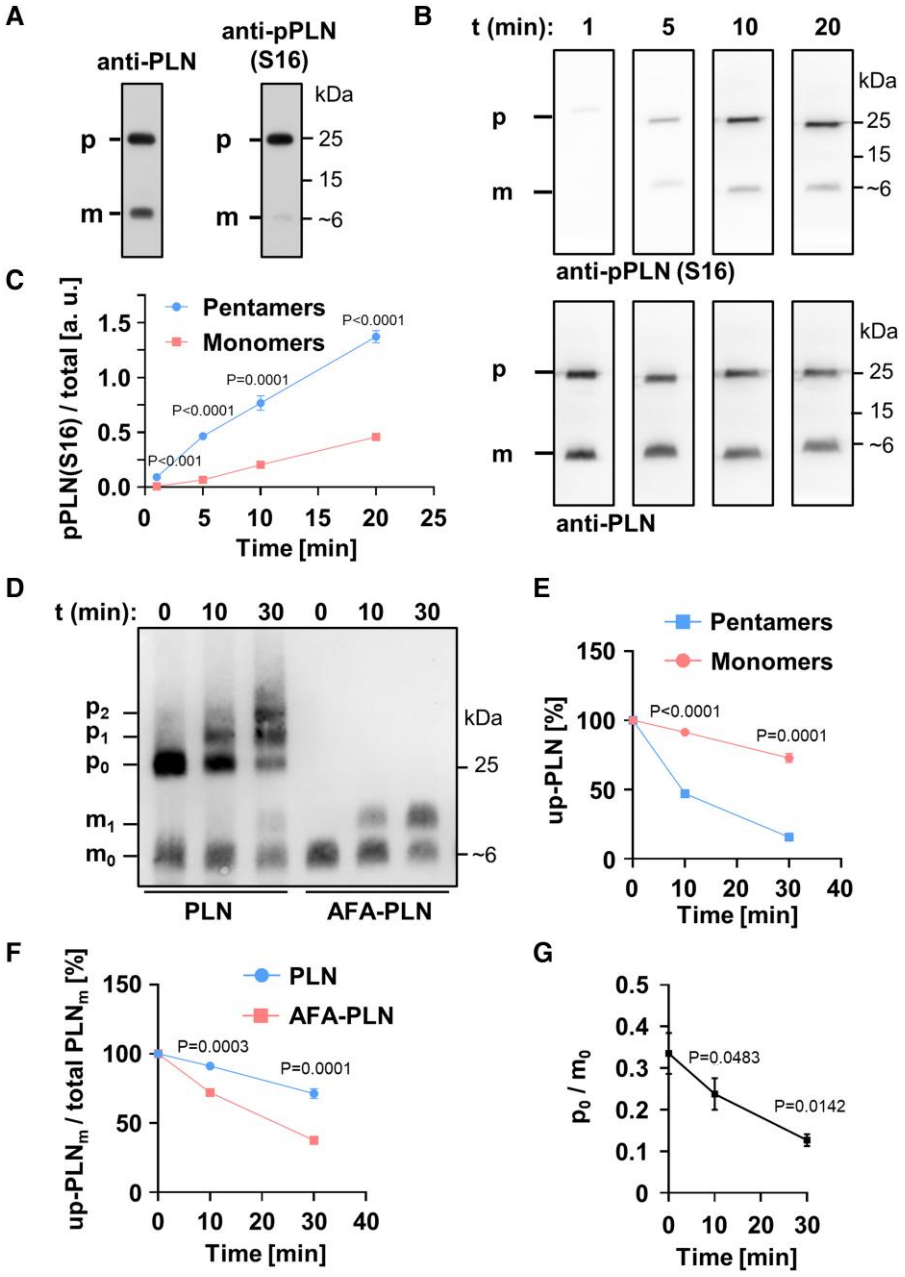

Figure 1 Phospholamban (PLN) pentamers are excellent protein kinase A (PKA) substrates. (*A*) SDS-PAGE and western blot using mouse heart lysates probed with antibodies against total PLN (left) or PLN phosphorylated at S16 (right). (*B*) Far western kinase assay; phosphorylation of separated and fixed pentamers and monomers with PKA; antibodies as in (*A*). Heart lysates were dephosphorylated prior to separation and fixation of PLN monomers and pentamers on polyvinylidene difluoride membrane. After renaturation, pentamers and monomers were phosphorylated with PKA for 1, 5, 10, or 20 min. (*C*) Quantification of (*B*); shown are the mean signal intensities of PKA-dependent monomer/pentamer phosphorylation at S16. Phosphorylation signals of monomers and pentamers were normalized to the respective total PLN signal intensities. Mean ± SEM, $N = 8$ hearts, two-way ANOVA followed by Sidak's multiple comparisons test. (*D*, *E*) *In vitro* phosphorylation of synthetic PLN (adjusted for equal monomer amounts) by PKA for 0, 10, and 30 min in solution followed by western blot using Phos-tag™-gels and anti-PLN antibodies; m_x, p_x: Monomers (pentamers) with $x = 0$, 1, 2 phosphate group(s); up-PLN, unphosphorylated PLN. Note the strong phosphorylation of pentamers ($p_1 + p_2$) compared to monomers (m_1) for wild-type PLN (PLN). Mean ± SEM, $N = 6$, pentamers and monomers compared by two-way ANOVA followed by Sidak's multiple comparisons test. (*F*) PLN monomer depletion during PKA-dependent phosphorylation comparing wild-type PLN and AFA-PLN as shown in (*D*); Mean ± SEM, $N = 6$, two-way ANOVA followed by Sidak's multiple comparisons test. (*G*) Molar substrate ratios of unphosphorylated pentamers (p_0) and monomers (m_0) as quantified from (*D*). Mean ± SEM, $N = 6$, repeated measures one-way ANOVA followed by Tukey's multiple comparisons test vs. t_0.

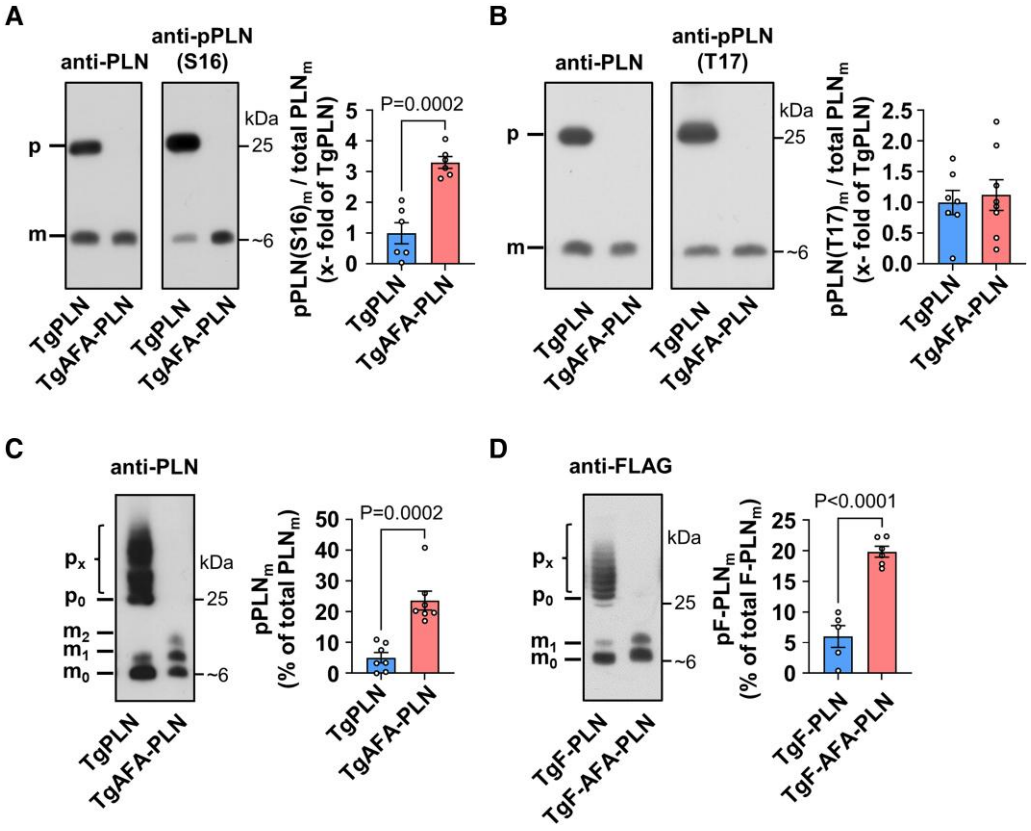

Figure 2 Phosphorylation of phospholamban (PLN) monomers in heart tissue is reduced if PLN can form pentamers. (*A*, *B*) Western blot using antibodies against PLN phosphorylated at S16 [anti-pPLN(S16)], T17 [anti-pPLN(T17)], and total PLN (anti-PLN); heart tissue was quickly harvested from mice after anaesthesia for 20 min; for comparison of monomer phosphorylation under equal conditions, total protein loads were lower for TgAFA-PLN (2.2-fold) to match the amounts of total PLN monomers in SDS gels; *m*, monomers (~6 kDa); *p*, pentamers (~25 kDa); bar graph shows proportion of S16-(T17-)phosphorylated PLN monomers ($pPLN(S16/T17)_m$) relative to total PLN monomers (PLN_m); $N = 6–7$ hearts per group. (*C*, *D*) Western blot using Phos-tag™-gels; graphs show percentage of phosphorylated PLN monomers ($pPLN_m$); (*C*) heart lysates as in *A* and anti-PLN antibodies; $N = 7$ hearts per group; (*D*) heart lysates of independent mouse lines expressing PLN and AFA-PLN transgenes tagged with a FLAG epitope at the *N*-termini (TgF-PLN and TgF-AFA-PLN); tagged protein was detected by anti-FLAG antibodies; m_x, p_x, monomers (pentamers) with $x = 0–10$ phosphate group(s); groups were compared by unpaired two-tailed Student's *t* test.

cervical dislocation, and stored at −80°C until further processing. To obtain heart tissue after intensive stimulation of β-adrenergic receptors, the protocol was identical, but 5-µg isoproterenol in 100-µL saline were injected intraperitoneally 3 min before harvest of hearts.

2.8 Immunoblot detection of proteins

Snap-frozen heart tissue was stored at −80°C until mechanical lysis (Ultra-Turrax® T10 basic, Ika®) in modified RIPA buffer (10 mM Tris/HCl pH 8.0, 0.5 mM EGTA, 0.5% Triton™ X-100, 0.1% deoxycholic acid, 0.1% SDS, and 140 mM NaCl) supplemented with protease inhibitors and phosphatase inhibitors. If not stated otherwise, equal amounts of total protein (Pierce® BCA Assay Kit, ThermoScientific) were separated on 15% polyacrylamide gels and transferred to Immobilon-P polyvinylidene difluoride (PVDF) membranes (Millipore) before blocking unspecific binding with 0.5% milk/TBS-T [SNAP i.d.® 2.0, Millipore] and incubation with primary antibodies in TBS-T (10 mM Tris, 150 mM NaCl, 0.1% Tween 20, and pH 7.6) containing 5% milk overnight at 4°C. Reactive bands were visualized by chemiluminescence using secondary antibodies coupled to horse-radish peroxidase (Rockland) and Luminata Forte Western HRP substrate (Millipore). Unsaturated chemiluminescent signals were digitalized and quantified using a CCD camera system and associated software (ChemStudio, VisionWorks, AnalytikJena). The following antibodies were used for detection of proteins: anti-SERCA2 (A010–20, Badrilla, 1:5000 dilution), anti-PLN (clone A1, Badrilla, 1:5000 dilution), anti-phospho-PLN (S16) (Badrilla, 1:5000 dilution), anti-phospho-PLN (T17) (Badrilla, 1:5000 dilution), anti-FLAG (clone M2, Sigma, 1:10 000 dilution), anti-Troponin-I (#4002, Cell Signaling Technology, 1:2000 dilution), anti-phospho-Troponin-I (S23/24) (#4004, Cell Signaling Technology, 1:2000 dilution), anti-RyR2 (clone 34C, Thermo Fisher Scientific, 1:5000 dilution), anti-phospho-RyR2(S2808) (A010–30, Badrilla, 1:5000 dilution), HAX-1 (clone 52/HAX-1, BD Transduction Laboratories, 1:5000 dilution), Calsequestrin (PA1–913, Thermo Fisher Scientific, 1:5000 dilution), S100A1 (Acris, 1:5000 dilution), and Phospho-(Ser/Thr) PKA Substrate antibody (#9621, Cell Signaling Technology, 1:1000 dilution). Immunoblot analyses with and without PKA-dependent PLN phosphorylation demonstrated high specificity of anti-phospho-PLN (S16) antibodies for phosphorylated PLN (*Figure 1B* and Supplementary material online, *Figure S7C*).

2.9 Phosphate affinity SDS-PAGE

Phosphorylation patterns of PLN were further analysed by phosphate affinity SDS-PAGE. Protein was separated on 12.5% polyacrylamide gels containing 17.5 µM Phos-Tag™ acrylamide and 35 µM $MnCl_2$ according to the manufacturer's protocol (AAL-107, Wako Pure Chemical Industries, Ltd.).

Manganese was removed by incubation of gels in blotting buffer (25 mM Tris, 150 mM glycine, and 20% methanol) plus 10 mM EDTA prior to immunoblotting and protein detection using anti-PLN or anti-FLAG antibodies as described above.

2.10 Generation, solubilization, and phosphorylation of synthetic PLN

Synthetic PLN and PLN-AFA were generated by Fmoc solid-phase synthesis (Pepscan, Lelystad, NL). Successful synthesis of the correct product was verified by mass spectrometry. Synthetic PLN and AFA-PLN were resuspended in solubilization buffer [50 mM Tris (pH 7.5), 100 mM NaCl, 2 mM DTT, 10% glycerol, 0.5% Triton™ X-100] at a final concentration of 1 mg/mL and incubated at room temperature for 2 h. Solubilized synthetic PLN was phosphorylated with cAMP-dependent protein kinase (PKA) catalytic subunit (New England BioLabs) in the presence of 10 mM $MgCl_2$ and 200 μM ATP at 30°C. PKA reactions were stopped by adding 3 × SDS-PAGE sample buffer [50 mM Tris (pH 6.8), 0.6% SDS, 30% glycerol, 0.015% bromophenol blue].

2.11 Far western kinase assay

Heart ventricle homogenates were dephosphorylated with lambda protein phosphatase (400 U, New England BioLabs) for 30 min at 30°C in the presence of 1 mM $MnCl_2$ prior to the experiments. Separation and phosphorylation of PLN monomers and pentamers were essentially performed as described by Wu *et al.*,[23] but denaturation steps by guanidine hydrochloride were omitted. Briefly, PLN monomers and pentamers were separated by SDS-PAGE and blotted to PVDF membrane as described above. Membranes were incubated in AC buffer [10% glycerol, 100 mM NaCl, 20 mM Tris (pH 7.5), 1 mM EDTA, 0.1% Tween-20, 2% milk powder, and 1 mM DTT] for 45 min before blocking with TBS-T containing 5% milk for 1 h. PKA phosphorylation of membrane-bound protein was carried out at 30°C in PKA reaction buffer (50 mM HEPES, 10 mM $MgCl_2$, 200 μM ATP, and pH 7.5) with 0.5 U/μL PKA catalytic subunit (New England BioLabs). Reactions were stopped by washing the membranes with TBS-T prior to immunodetection of total and S16-phosphorylated PLN.

2.12 RNA preparation and real-time PCR

RNA was isolated from mouse ventricular heart tissue (RNeasy Midi Kit, Qiagen) to obtain total RNA followed by reverse transcription using oligo$(dT)_{12–18}$ primers and Superscript II reverse transcriptase (Invitrogen). cDNA of the following genes was amplified using the StepOnePlus RealTime PCR System (Thermo Fisher Scientific), HotMaster Taq DNA Polymerase (5 Prime, Quanta Bio), and the following primer pairs: PLN and AFA-PLN transgene, forward primer 5′-CTCCAGAACCTATT TATCAATTT-3′, reverse primer 5′-TGCCACCCATCAAGCTTAG TCAGA-3′; Glyceraldehyde-3-phosphate dehydrogenase (*Gapdh*), forward primer 5′-TGGCAAAGTGGAGATTGTTG-3′, reverse primer 5′-CATT ATCGGCCTTGACTGTG-3′. *Gapdh* expression was determined to normalize data. Quantitative real-time PCR results were analysed as described.[24]

2.13 Statistical analysis

If not stated otherwise, differences between more than two study groups were assessed using ANOVA, followed by Sidak's test for multiple comparisons, unpaired Student's *t* tests for comparisons of two groups, and log-rank test for comparison of survival curves. Data are presented as mean ± standard error (SEM), if not noted otherwise.

3. Results

3.1 PKA directly phosphorylates PLN pentamers

PLN pentamers are strongly phosphorylated in heart tissue (*Figure 1A*). We first wanted to know whether this results exclusively from oligomerization of phosphorylated monomers or if direct interaction of PLN pentamers with PKA, the principal kinase of PLN under β-adrenergic stimulation, can add to this phosphorylation pattern.

To answer this question, we adapted the method of far western blots, a technique that enables analysis of protein–protein interactions on a protein-binding membrane.[23] We completely dephosphorylated mouse ventricular homogenates by phosphatase treatment and used SDS-PAGE to separate PLN monomers and pentamers because PLN oligomeric states are known to closely resemble those found in lipid bilayers in SDS-containing solutions.[3] After separation, pentamers and monomers were blotted on PVDF membrane, thus preventing any exchange between pentamers and monomers during or after the subsequent phosphorylation with PKA (*Figure 1B*). Productive interaction of the kinase with its substrate was quantified by analysing PKA-dependent phosphorylation at S16 relative to total PLN (*Figure 1C*). Clear phosphorylation at S16 of both monomers and pentamers was detected in a time-dependent manner indicating that phosphorylation of PLN pentamers can indeed arise from direct phosphorylation and not exclusively from oligomerization of phosphorylated monomers. Furthermore, phosphorylation signals of pentamers increased at a higher rate than those of monomers arguing that pentamers constitute a preferred substrate for PKA.

To investigate if preferential pentamer phosphorylation is also observed with solubilized PLN, we then phosphorylated PLN with PKA for different durations, and the resulting phosphorylation was analysed using Phos-Tag™ gels that allow for electrophoretic separation of PLN species owing to their phosphorylation status (*Figure 1D*). To exclude any influence of protein interaction partners other than PKA, we used purified PKA catalytic subunit and synthetic full-length proteins of PLN in these experiments. Consistent with the results obtained using far western blot kinase assays (*Figure 1B* and *C*), we observed a faster increase of pentamers carrying one or two phosphates (p1 + p2) than phosphorylated monomers (m_1; left three lanes of *Figure 1D*; Supplementary material online, *Figure S16A*). Concordantly, the amount of unphosphorylated pentamers decreased at a higher rate than the amount of unphosphorylated monomers (*Figure 1E*; Supplementary material online, *Figure S15*). Quantitative data shown in Figure *1E* are presented as percent unphosphorylated of total monomers or pentamers, respectively, to take into account that pentamers provide five times more PKA phosphorylation sites than monomers.

Since phosphorylated monomers have an increased tendency for oligomerization,[9] we next evaluated to what extent phosphorylation of PLN monomers would increase the ratio of pentamers to monomers and thus contribute to the strong phosphorylation of pentamers observed in *Figure 1D* and *E*. To this end, synthetic PLN was phosphorylated by addition of PKA and ATP before addition of SDS in order to stop the reaction and to allow oligomerization for 0, 10, or 60 min (see Supplementary material online, *Figure S1*). The pentamer/monomer ratio of phosphorylated PLN remained unchanged within 10 min and also was unchanged compared to unphosphorylated PLN in SDS. In contrast, after 60 min a two-fold increase of the pentamer/monomer ratio was detected if PLN was phosphorylated, whereas unphosphorylated control samples still showed no change. These experiments demonstrated that phosphorylation-dependent changes of pentamer/monomer ratios would occur only later than 10 min in SDS-containing solution, which is longer than sample handling prior to SDS-PAGE in our experiments. These results are also in line with previous reports that found no subunit exchange between monomer and pentamers in membranes of live cells during an observation period of 80 s, and only limited capacity of pentamers to buffer the concentration of PLN monomers.[15,25]

3.2 PLN pentamers and monomers compete for PKA

We next wanted to know if the strong and direct phosphorylation of PLN pentamers leads to competition with monomers for PKA. Therefore, we analysed the phosphorylation patterns of PLN monomers in SDS under conditions that either allowed or prevented pentamerization. To exclude any influence of protein interaction partners other than PKA, we again

used purified PKA catalytic subunit and synthetic full-length PLN and compared it to AFA-PLN, a well characterized fully functional monomeric variant of PLN.[26–28] In AFA-PLN, oligomerization is prevented by substitution of three cysteine residues in the transmembrane region of the wild-type protein. Nevertheless, the cytosolic domains of AFA-PLN (that harbour all phosphorylation sites[29]) have the same conformation as monomeric wild-type PLN. None of the three mutations alters the inhibitory function on SERCA2a as compared to wild-type PLN monomers.[5] Also, phosphorylation kinetics are identical to that of PLN monomers as confirmed by far western blot kinase assays (see Supplementary material online, *Figure S2*). In contrast, AFA-PLN phosphorylation in solution was clearly stronger than that of PLN monomers (with the ability to form pentamers) (*Figure 1D*; Supplementary material online, *Figure S16B*). As detailed above and shown in Supplementary material online, *Figure S1*, weak phosphorylation of PLN monomers in these experiments cannot be caused by pentameric assembly of phosphorylated monomers or their exchange against unphosphorylated protomers. Importantly, the amount of unphosphorylated AFA-PLN also decreased at higher rate than unphosphorylated PLN monomers (m_0) demonstrating that PKA substrates, i. e. unphosphorylated PLN monomers, are utilized more readily in the absence of pentamers (*Figure 1F*, $P < 0.001$). These results are consistent with competition of PLN pentamers and monomers for PKA and with recent findings by mathematical modelling that showed substrate competition with PLN pentamers to be sufficient to explain delayed phosphorylation of PLN monomers.[15]

To further characterize the competition between unphosphorylated pentamers and monomers for PKA, we sought to compare the specificity of the enzyme for either substrate. Since pentamers and monomers cannot be separated in solution, enzyme kinetic parameters cannot readily be determined individually for each substrate. However, substrate specificity for any competing pair of substrates can be assessed by the measurement of relative substrate depletion that reflects the ratio of specificity constants k_{cat}/K_m (turnover number/Michaelis constant).[30,31] We found that relative substrate depletion, i. e. the molar ratio of unphosphorylated pentamers to monomers (p_0/m_0), decreases strongly upon phosphorylation suggesting higher substrate specificity of PKA for pentameric PLN (*Figure 1G*).

3.3 PLN pentamerization results in reduced S16 phosphorylation of PLN monomers in heart tissue

PLN pentamers turned out as excellent PKA substrates of PKA that reduce S16 phosphorylation of monomers, the active PLN species (*Figure 1B–E*). To further investigate these findings and its functional consequences in whole hearts, we generated mouse models with and without the ability to form PLN pentamers. Wild-type PLN or oligomer-deficient AFA-PLN was expressed in mouse hearts under the control of the α-cardiac myosin heavy chain promoter (see Supplementary material online, *Figure S3A*). Two mouse lines with similar expression levels of transgenes were crossed with PLN-deficient mice (PLN-KO) to obtain animals that expressed transgenic but no endogenous PLN, designated TgPLN and TgAFA-PLN (see Supplementary material online, *Figure S3B*). TgPLN expressed 1.19 ± 0.08-fold more PLN than strain-matched wild-type mice (P = NS). Cardiac morphology and function of TgPLN *in vivo* were indistinguishable from age- and strain-matched wild-type mice (see Supplementary material online, *Table S1*, Supplementary material online, *Figure S4*). TgAFA-PLN expressed 13% less total PLN than TgPLN ($P = 0.21$) but 2.22 ± 0.10-fold more PLN monomers on SDS-PAGE ($P < 0.001$; Supplementary material online, *Figure S3C and D*). Using these mouse lines ruled out lower amounts of the inhibitory PLN species, i. e. PLN monomers, in TgAFA-PLN compared to TgPLN hearts, even if the latter would form less PLN pentamers during experiments *in vivo* and *in vitro* than on SDS gels. There were no indications for morphological abnormalities or heart failure in both mouse lines within the observation period of one year (see Supplementary material online, *Figure S5*, Supplementary material online, *Table S2 and S3*).

To investigate the phosphorylation status of PLN monomers independent of potentially fluctuating sympathetic activity, mice were anaesthetized for 20 min prior to harvest of hearts. Equal amounts of monomeric PLN species were loaded onto the gels, and the ratio of signal intensities phospho/total was calculated for each sample. Monomer phosphorylation was ~3 times stronger in the absence of PLN pentamers (TgAFA-PLN, $P < 0.001$), suggesting that PLN pentamerization reduces the basal phosphorylation state of the monomer pool in mouse hearts (*Figure 2A*). In contrast to the weak monomer phosphorylation, TgPLN demonstrated marked S16 phosphorylation of PLN pentamers. Unlike S16, immunoblot analyses detected no differences of PLN phosphorylation at T17 in mouse hearts that were beating until they were snap-frozen, suggesting that pentamerization only affects PKA-dependent phosphorylation (*Figure 2B*).

The phosphorylation patterns of PLN monomers were further investigated independently of phospho-specific antibodies using Phos-tag™ gels to determine the ratio of phosphorylated to unphosphorylated PLN species. These analyses yielded four to five times more phosphorylated monomers if pentamers were depleted ($P < 0.001$; *Figure 2C*), indicating that PLN pentamerization also reduces baseline monomer phosphorylation in heart tissue. These findings were further confirmed in two independent transgenic mouse lines expressing N-terminally tagged PLN or AFA-PLN (TgF-PLN and TgF-AFA-PLN) for detection independent of anti-PLN antibodies (*Figure 2D*). Phosphorylation of PLN monomers was also low in TgPLN and strong in TgAFA-PLN if mice were resting (but were not anaesthetized) before harvest of hearts (see Supplementary material online, *Figure S6*).

3.4 PLN pentamerization extends the range of monomer phosphorylation

We next investigated the phosphorylation patterns of PLN after intraperitoneal application of 5 μg isoproterenol to induce maximal PKA stimulation. Cardiac β-adrenergic receptor stimulation was monitored by the increase of heart rate, which was maximal three minutes after injection. Thus, this time point was chosen to quickly harvest and snap-freeze the mouse hearts. Immunoblot analyses demonstrated largely enhanced phosphorylation of both PLN monomers and pentamers (*Figure 3A* and *B*). Importantly, the intensity of monomer phosphorylation was comparable in TgPLN and TgAFA-PLN indicating that PLN pentamers do not compromise phosphorylation of monomers under conditions of intense kinase activation.

The stoichiometry of pentamer and monomer phosphorylation was evaluated by Phos-tag™-SDS-PAGE (*Figure 3C*). Quantitative analysis demonstrated that under basal conditions (20 min anaesthesia of mice), PLN monomers are essentially dephosphorylated (94.6 ± 2.9%) while a significant proportion of pentamers is phosphorylated. By comparison, in resting mice that did not receive anaesthesia, only 56.4 ± 3.1% of PLN monomers were dephosphorylated and the majority of phosphorylated monomers carried one phosphate. Finally, isoproterenol induced phosphorylation of >80% of PLN monomers, a majority of them even carried two phosphate groups indicating that adrenergic stimulation is perfectly capable of monomer phosphorylation if PLN is able to form pentamers. Since PLN monomer phosphorylation is three- to four-fold stronger in TgAFA-PLN compared to TgPLN under basal conditions (*Figure 2*), we conclude that near-complete dephosphorylation of PLN monomers and thereby maximum SERCA2a inhibition can only be achieved in the presence of pentamers. Thus, pentamerization extends the range of possible PKA-dependent phosphorylation states of PLN monomers.

3.5 PLN pentamerization alters the activity of the Ca^{2+}-ATPase

PLN monomers inhibit SERCA2a by direct interaction in dependence on their phosphorylation state. We thus analysed the functional consequences arising from the observed differences of PLN monomer phosphorylation in TgPLN and TgAFA-PLN. Ca^{2+} transients were measured in isolated and electrically paced cardiomyocytes (0.5 Hz) of 8 to 10-week-old mice using the fluorescent Ca^{2+} indicator Fura-2 (*Figure 4A*, Supplementary material online, *Table S4*). Under basal conditions, we

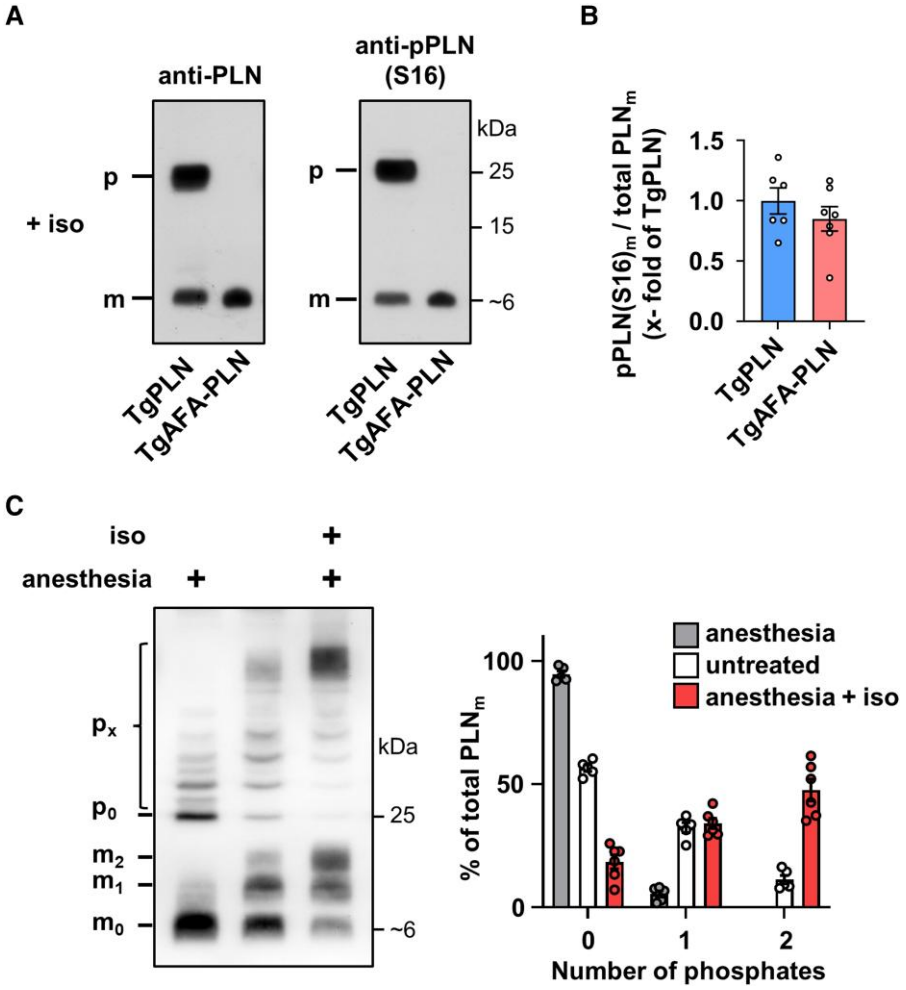

Figure 3 Phospholamban (PLN) pentamers allow for strong monomer phosphorylation upon PKA activation. (*A*) Western blot of TgPLN and TgAFA-PLN mouse heart ventricular tissue for phosphorylated PLN [anti-pPLN(S16)] and total PLN (anti-PLN) after isoproterenol stimulation (5 μg i.p.) of mice for 3 min; total protein loads were lower for TgAFA-PLN (2.2-fold) to obtain equal amounts of total PLN monomers in SDS gels; (*B*) Quantitative analysis of S16-phosphorylated monomers ($pPLN(S16)_m$), $N = 6$ TgPLN and 7 TgAFA-PLN hearts; groups were compared by Student's *t* test. (*C*) Phosphate affinity SDS-PAGE (Phos Tag™) to separate monomeric and pentameric PLN species according to their phosphorylation status (m_x, p_x: monomers (pentamers) with *x* phosphate group(s). Heart lysates were compared between anaesthetized (left), untreated (middle) or isoproterenol-treated mice (right, iso, 5 μg i.p.) using anti-PLN antibodies. Quantification shows the relative proportion of PLN monomers carrying 0, 1, or 2 phosphate groups. $N = 6$ hearts per group.

found accelerated cytosolic Ca^{2+} elimination in TgAFA-PLN compared to TgPLN myocytes (3.5 ± 0.5 ΔF/s vs. 2.1 ± 0.2 ΔF/s, $P < 0.05$; *Figure 4A* and *B*). To exclude the possibility that the observed differences are based on inherent inhibitory differences independent of PLN phosphorylation in TgPLN and TgAFA-PLN, we also measured Ca^{2+} transients in cells treated with the PKA inhibitor H-89. Treatment with H-89 resulted in a reduction of S16 phosphorylation below detection limits, while Ca^{2+} transient kinetics became indistinguishable between TgPLN and TgAFA-PLN (see Supplementary material online, *Figure S7*, Supplementary material online, *Table S5*), indicating that the different effects on Ca^{2+} handling measured in the experiments shown in *Figure 4* are PKA-dependent. Importantly, we found no differences between TgPLN and TgAFA-PLN hearts with regard to the expression and phosphorylation of ryanodine receptor and troponin I, PLN-T17 phosphorylation, and the expression of SERCA2a, HAX-1 and S100A1 (see Supplementary material online, *Figure S8*). Thus, we concluded that the observed Ca^{2+}-dependent effects mostly hinge on the phosphorylation of PLN at S16, i. e. stronger basal monomer phosphorylation in TgAFA-PLN than in TgPLN hearts. Adrenergic receptor stimulation by isoproterenol (10^{-7} M) accelerated Ca^{2+} cycling of cardiomyocytes. However, unlike basal Ca^{2+} kinetics, under these conditions, the speed of cytosolic Ca^{2+} elimination was not different between TgAFA-PLN and TgPLN cells (*Figure 4D*).

Taken together, PLN pentamerization is necessary to reduce diastolic SR Ca^{2+} transport by SERCA2a under basal conditions, but it does not restrict the inactivation of PLN inhibitory function upon β-adrenergic stimulation. Thus, the possibility for PLN to form pentamers seems to broaden the limits within which PKA can modify SERCA2a activity and diastolic Ca^{2+} kinetics.

3.6 PLN pentamerization extends the dynamic range of cardiac relaxation

Changes of cytosolic Ca^{2+} concentrations coordinate sarcomere contraction and relaxation. To assess the consequences of the distinct Ca^{2+}

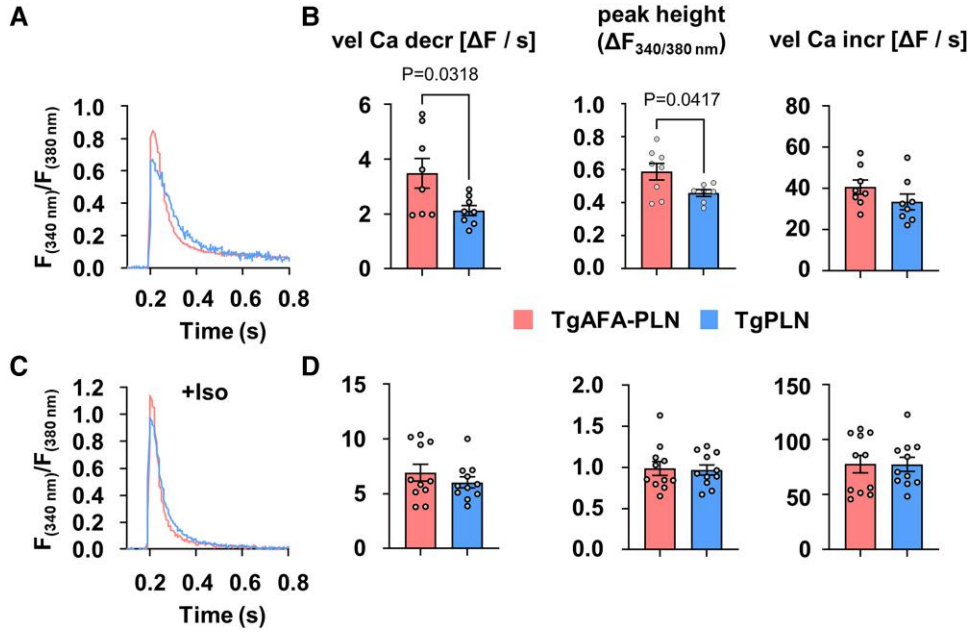

Figure 4 Basal cardiomyocyte sarco/endoplasmic reticulum (SR) Ca^{2+} uptake rates are reduced if phospholamban (PLN) can form pentamers. Measurements of Ca^{2+} transients in isolated and electrically paced cardiomyocytes (0.5 Hz) of TgPLN and TgAFA-PLN mice. (*A*, *C*) Representative recordings at baseline (*A*) and after stimulation with 10^{-7} M isoproterenol (Iso, *C*). (*B*, *D*) Quantitative data show the height of Ca^{2+} transient amplitudes (maximum change in fluorescence, ΔF, at wave lengths 340/380 nm) and the velocities of Ca^{2+} transient increase (vel Ca incr) and decrease (vel Ca decr). Each data point represents the averaged values from ∼10 myocytes per heart and ∼10 Ca^{2+} transients per myocyte; $N = 8–11$ hearts and 76–105 cells per group, comparison of groups by unpaired two-tailed Students *t* test.

handling in TgAFA-PLN and TgPLN myocytes on sarcomere function, we measured the kinetics of sarcomere mechanics in paced cardiomyocytes (*Figure 5*; Supplementary material online, *Table S6*). Compared to TgPLN, sarcomere contraction and relaxation were faster in TgAFA-PLN. β-Adrenergic receptor stimulation by 10^{-7} M isoproterenol completely abrogated these differences due to stronger enhancement of sarcomere function in TgPLN (*Figure 5B* and *C*). Of note, isoproterenol also induced a significant increase of the contractile amplitude only in TgPLN.

We further assessed the impact of PLN pentamerization on whole heart myocardial function *in vivo* by left ventricular catheterization of TgPLN, TgAFA-PLN, and PLN-KO mice that served as controls (*Figure 6*). The speed of left ventricular pressure decay (dp/dt_{min}) was slowest in TgPLN at baseline (-5332 ± 422 mmHg/s vs. -6343 ± 247 mmHg/s in TgAFA-PLN and -6936 ± 391 mmHg/s in PLN-KO; *Figure 6A*). Notably, dp/dt_{min} of TgAFA-PLN and PLN-KO mice were not significantly different. Upon stimulation of β-adrenergic receptors by intravenous infusion of β-adrenergic receptor agonist dobutamine at increasing concentrations, the acceleration of dp/dt_{min} was stronger in TgPLN than in TgAFA-PLN and PLN-KO hearts indicating higher sensitivity of ventricular relaxation to adrenergic stimulation (*Figure 6A*). At high doses of dobutamine, dp/dt_{min} of TgPLN and TgAFA-PLN mice were almost as fast as that of PLN-KO hearts indicating near-complete PLN inactivation.

LV pressure rise (dp/dt_{max}) was faster in PLN-KO than in TgPLN at baseline (8641 ± 503 vs. 6608 ± 616 mmHg/s, $P < 0.05$; *Figure 6B*), concordant with hypercontractility described for PLN-KO animals.[32] In contrast, dp/dt_{max} of PLN-KO was not significantly higher compared to TgAFA-PLN (7412 ± 503 mmHg/s). Upon dobutamine stimulation, dp/dt_{max} was identical in all three mouse lines. Maximum LV pressure (LVP_{max}) and heart rates were not different among groups at baseline nor upon dobutamine stimulation (see Supplementary material online, *Figure S9*).

Taken together, the functional characterization demonstrated slow cytosolic Ca^{2+} elimination and slow myocardial relaxation in the presence of pentamers under resting conditions. β-Adrenergic receptor activation can overcome this inhibition and almost fully inactivate PLN thereby increasing the regulatory bandwidth of cardiac relaxation.

3.7 PLN pentamerization improves myocardial adaptation to pressure overload

Basal phosphorylation of PLN monomers is reduced if PLN can oligomerize leading to high inhibitory activity but still allows strong phosphorylation and near-complete inactivation of PLN monomers upon β-adrenergic receptor stimulation (*Figures 2–4*). PLN phosphorylation by PKA due to β-adrenergic receptor activation represents a predominant response mechanism to changes in cardiac workload. Thus, we hypothesized that PLN pentamerization may play a relevant role in myocardial adaptation to cardiac stress since it enhances the sensitivity and dynamic range of myocyte Ca^{2+} regulation and relaxation. To test this, we compared survival, cardiac remodelling and left ventricular haemodynamics of TgPLN, TgAFA-PLN, and PLN-KO mice subjected to TAC that imposes chronic pressure overload on the heart.

Left ventricular pressure overload did not affect the ability of PLN to form pentamers. Enhanced phosphorylation rates and preferential phosphorylation of PLN pentamers by PKA were also observed 1 week after TAC (see Supplementary material online, *Figure S10* and *S11*). Phosphorylation of PLN monomers was still three- to four-fold stronger in the absence of pentamers (see Supplementary material online, *Figure S12*). TAC also did not significantly alter the expression and activity of the central Ca^{2+} cycling proteins, RyR2, and SERCA2a, compared to baseline values, and SERCA2a/PLN ratios were unchanged (see Supplementary material online, *Figure S12*). Within the first 4 weeks after TAC, survival of TgPLN mice was significantly higher compared to

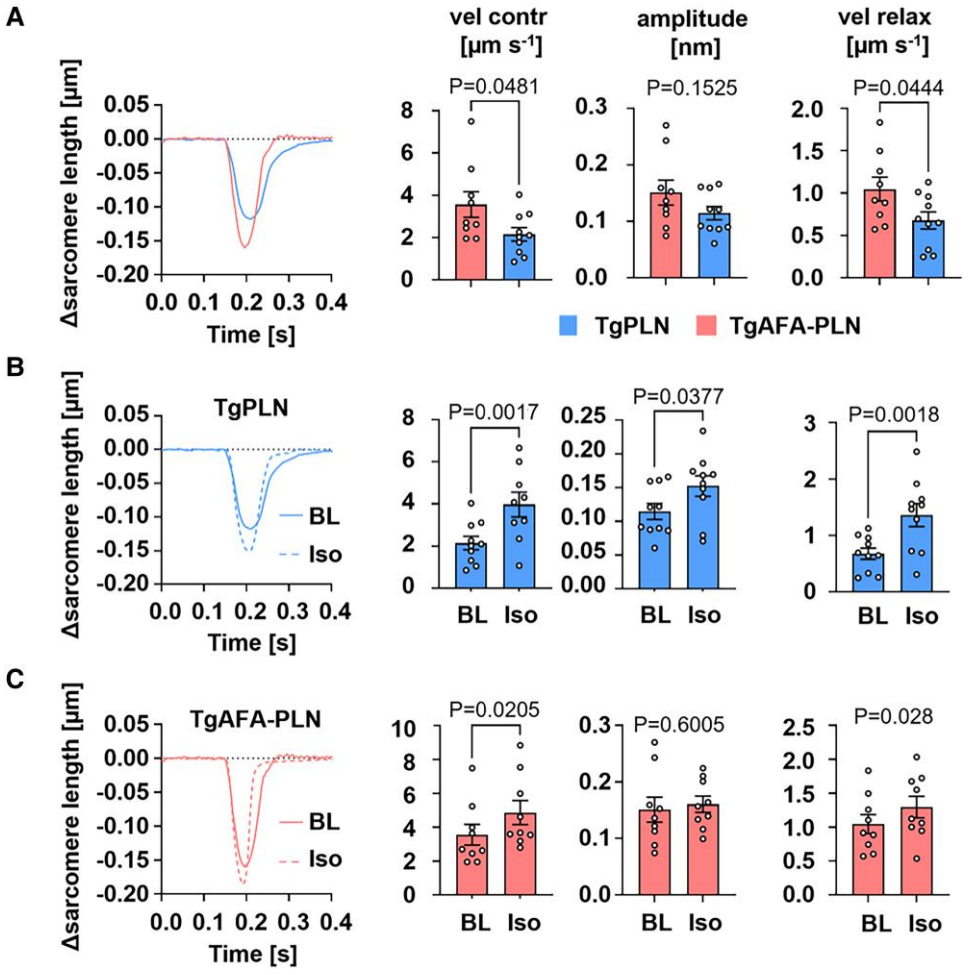

Figure 5 Extended dynamic range of sarcomere contraction and relaxation if PLN can form pentamers. Measurements of sarcomere length during electrical pacing (0.5 Hz) of cardiomyocytes isolated from TgPLN and TgAFA-PLN hearts. (*A*) Representative baseline recordings during a cycle of contraction and relaxation; sarcomere kinetics were measured without (BL) and with stimulation with 10^{-7} isoproterenol (Iso) for TgPLN (*B*) and TgAFA-PLN (*C*); vel contr, velocity of sarcomere contraction; amplitude, change of sarcomere length upon stimulation; vel relax, velocity of sarcomere relaxation. $N = 9–16$ hearts and 75–123 cells per genotype; unpaired (*A*) and paired (*B*, *C*) two-tailed Students *t* test.

TgAFA-PLN and PLN-KO animals (log-rank test, $P < 0.05$; *Figure 7A*). Echocardiography 7 weeks after TAC revealed that fractional shortening of surviving mice was lower in PLN-KO hearts (27 ± 1%) than in TgAFA-PLN (37 ± 2%, $P < 0.01$) and TgPLN (44 ± 2%, $P < 0.0001$) hearts (*Table 1*). Accordingly, systolic left ventricular volumes were 27 ± 3 µL in PLN-KO, 19 ± 2 µL in TgAFA-PLN, and only 11 ± 2 µL in TgPLN ($P <$ 0.001 vs. PLN-KO and 0.08 vs. TgAFA-PLN) indicating dilation of left ventricular chambers in PLN-KO and to a lesser extent in TgAFA-PLN compared to TgPLN mice. Despite increased cardiac diameters, left ventricular wall thicknesses were comparable among all mouse lines suggesting excessive growth of cardiomyocytes that lack PLN pentamers (PLN-KO and TgAFA-PLN; *Table 1*).

LV mass was higher by trend in PLN-KO and TgAFA-PLN animals (*Table 1*), and heart weight was significantly higher than in TgPLN animals ($P < 0.05$, *Figure 7B*). Myocardial fibrosis of PLN-KO and TgAFA-PLN hearts was also increased after TAC compared to TgPLN hearts (PLN-KO, 4.8 ± 1.0%; TgAFA-PLN, 3.8 ± 0.4%; TgPLN, 1.7 ± 0.3%; $P < 0.05$, *Figure 7C* and *D*). Seven weeks after TAC, haemodynamic measurements were performed without and with dobutamine stimulation (1.5 µg/min i.v.) to analyse if PLN pentamerization enables a broader regulatory range of myocardial relaxation also in chronically pressure-overloaded hearts. In fact, β-adrenergic stimulation induced a significant decrease of dp/dt_{min} only in TgPLN, whereas TgAFA-PLN and PLN-KO hearts showed no change (TgPLN, −3240 ± 596 mmHg/s; TgAFA-PLN, 151 ± 505 mmHg/s; PLN-KO, −196 ± 465 mmHg/s, $P < 0.01$; *Figure 7E*).

Unlike TgPLN, dp/dt_{max}, LVP_{max}, and heart rate also showed a blunted response to β-adrenergic stimulation in TgAFA-PLN and PLN-KO. This inability of TgAFA-PLN and PLN-KO hearts to increase cardiac function above baseline levels contrasts with the haemodynamics of these mouse lines before TAC (*Figure 6*; Supplementary material online, *Figure S9*). The impaired responsiveness to β-adrenergic receptor stimulation, along with the increased mortality, adverse remodelling, LV dilation, and reduced contractility, suggests that PLN-KO and TgAFA-PLN hearts are more susceptible to cardiac stress and to the development of heart failure upon chronic pressure overload.

4. Discussion

The present study demonstrates that PLN pentamers are excellent and direct PKA substrates that compete with PLN monomers for free PKA (*Figure 1*). In fact, PKA favours pentamers over monomers leading to about

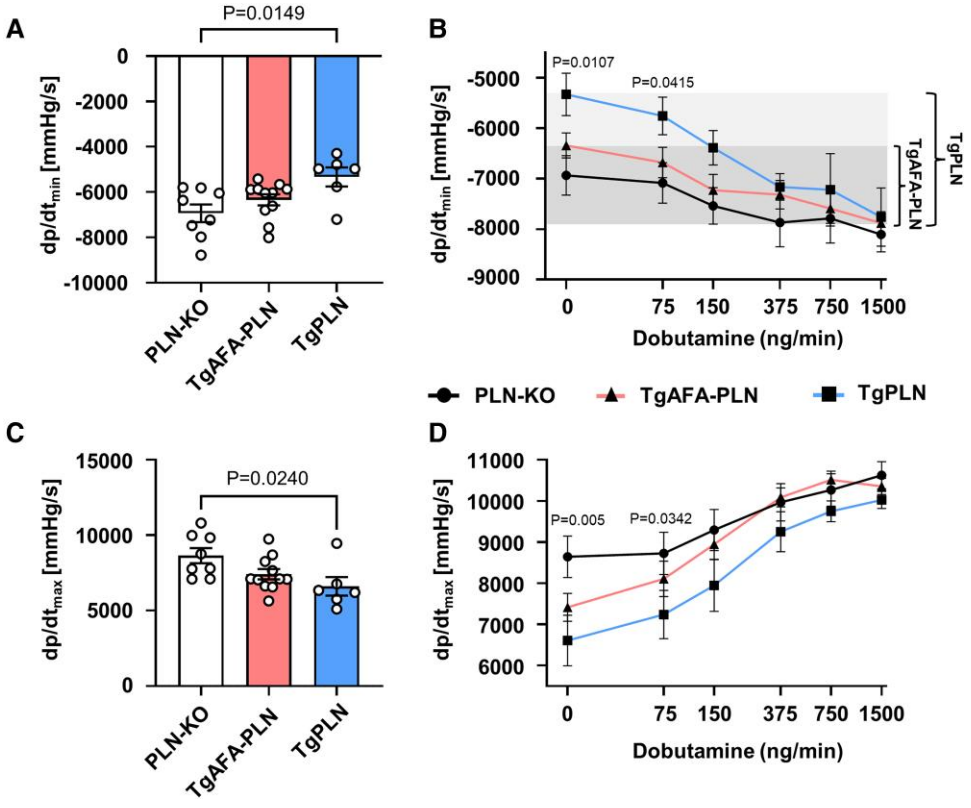

Figure 6 The sensitivity of cardiac function to β-adrenergic stimulation is enhanced if phospholamban (PLN) can form pentamers. Left ventricular haemodynamics of 8-week-old mice at baseline (*A*, *C*) and during intravenous application of dobutamine at increasing concentrations (*B*, *D*). Note the larger dynamic range of cardiac relaxation in TgPLN compared to TgAFA-PLN (shaded area); dp/dt_{min}, speed of left ventricular pressure decay; dp/dt_{max}, speed of left ventricular pressure rise; $N = 6–11$ mice per group; *P* values were determined by one-way ANOVA (*A*, *C*) and mixed-effects model (REML) comparing TgPLN to TgAFA-PLN and PLN-KO mice (*B*, *D*).

three-fold lower basal monomer phosphorylation compared to a situation when PLN pentamerization is prevented, as in TgAFA-PLN (*Figure 2*). This way, PLN pentamerization enhances monomer-driven SERCA2a inhibition, and slows down cytosolic Ca^{2+} clearance of cardiomyocytes, diastolic sarcomere relengthening and myocardial relaxation under basal conditions (*Figures 4–6*). Nevertheless, β-adrenergic receptor stimulation was able to fully reverse this inhibition by inducing strong phosphorylation both of PLN monomers and pentamers (*Figure 3*). Under these conditions, myocyte Ca^{2+} kinetics, sarcomere, and myocardial relaxation of hearts with and without PLN pentamerization were indistinguishable from each other and almost as fast as in PLN-KO hearts (*Figures 4–6*). Taken together, PLN pentamerization not only enhances the inhibition of SERCA2a at baseline, but also warrants good responsiveness of the heart to increased sympathetic tone. Thereby, PLN pentamerization increases the sensitivity and extends the regulatory range for modulation of SERCA2a activity, myocyte Ca^{2+} cycling, and cardiac relaxation. These characteristics of PLN pentamers may be causative for the better adaptation of TgPLN hearts to chronic pressure overload and therefore critical in conditions such as aortic stenosis or hypertensive heart disease (*Figure 7*, *Table 1*).

PLN monomers are known to represent the PLN species that directly inhibits SERCA2a,[5–8] in that they bind to a groove between four transmembrane helices of SERCA2a, thereby decreasing the Ca^{2+} affinity of the enzyme.[5,33,34] In contrast, after oligomerization, PLN is unable to bind to this regulatory interaction site.[10,11] PLN pentamers nevertheless play an active role in SERCA2a regulation and thus in cardiac function by impacting on the phosphorylation state of PLN monomers, as shown in the present study. The mitigation of monomer phosphorylation in the presence of pentamers at basal PKA activity explains previous findings of faster Ca^{2+} transient decline and faster cardiomyocyte relaxation in a mouse line expressing a monomeric PLN mutant.[35] The preferential phosphorylation of the pentameric form by PKA further demonstrates the impact of the oligomeric state of PLN on its interaction with other proteins. Apart from PKA and SERCA2a, pentamerization of PLN has been shown to affect the interaction with 14–3–3 proteins that preferentially bind to phosphorylated PLN pentamers, protecting pentamers from dephosphorylation and thereby adding another level of activity modulation.[36] Finally, PLN oligomers would enhance distinct phosphorylation states of monomeric and pentameric PLN since pentamer dephosphorylation occurs by a co-operative mechanism.[37]

To determine the functional implications of PLN pentamerization, the ideal model organisms would differ from each other exclusively by the presence or absence of PLN pentamerization. Our mouse lines TgPLN and TgAFA-PLN expressed either wild-type PLN or AFA-PLN that preferentially is monomeric. Both transgenes were controlled by the cardiomyocyte-specific α-MHC promoter in a genetic PLN null background. Limitations of these models would be differences in PLN monomer expression, which cannot be fully ruled out by western blot analyses (see Supplementary material online, *Figure S3*), because the latter may not reflect the actual pentamer-to-monomer ratios *in vivo*. Further, comparable SERCA2a affinity and inhibitory power of wild-type PLN monomers and AFA-PLN were only shown *in vitro*.[26–28] Thus, it was important to find that SERCA2a inhibition was the same in TgPLN and TgAFA-PLN if the transgenic proteins were unphosphorylated (see Supplementary material online, *Figure S7*, Supplementary material online,

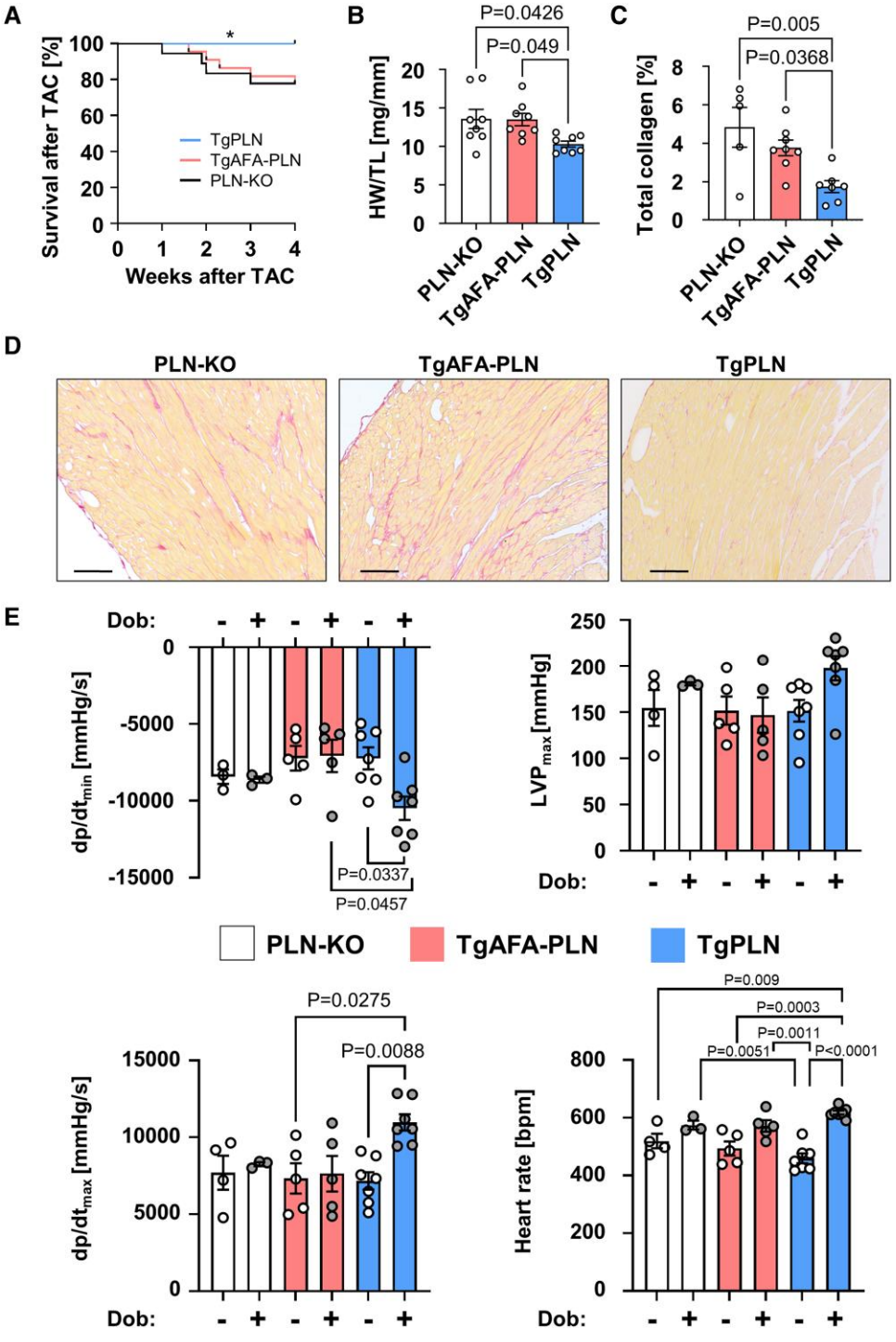

Figure 7 Phospholamban (PLN) pentamerization protects from pressure-overload induced heart failure. Seven weeks after transverse aortic constriction (TAC), TgPLN show longer survival, less interstitial collagen deposition, less left ventricular (LV) dilation, and better cardiac haemodynamics than TgAFA-PLN and PLN-KO. (*A*) Kaplan-Meier survival curves after TAC; log-rank test for TgPLN vs. TgAFA-PLN ($P = 0.0389$) and PLN-KO ($P = 0.042$). (*B*) Heart weight (HW) to tibia length (TL) ratios. (*C*, *D*) Representative histological pictures (scale bars 100 μm) and quantitative analysis of red staining in serial LV sections after Sirius Red staining. (*E*) Speed of LV pressure decay (dp/dt_{min}) and pressure rise (dp/dt_{max}), maximum pressure (LVP_{max}) and heart rate, as determined by LV catheterization of anaesthetized mice. Measurements were obtained before and after intravenous infusion of 1.5 μg/min dobutamine (Dob). Groups were compared by two-way ANOVA followed by Tukey's multiple comparisons test.

Table 1 Echocardiography 7 weeks after TAC

	PLN-KO	TgAFA-PLN	*P* vs. PLN-KO	TgPLN	*P* vs. PLN-KO	*P* vs. TgAFA-PLN
N	12	17		12		
Pressure gradient (mm Hg)	68 ± 7	73 ± 5	0.94	70 ± 7	0.96	0.81
LVAW;d (mm)	1.25 ± 0.02	1.32 ± 0.02	0.29	1.24 ± 0.05	0.99	0.26
LVPW;d (mm)	1.24 ± 0.03	1.29 ± 0.02	0.61	1.24 ± 0.05	0.99	0.54
LVID;d (mm)	3.60 ± 0.11	3.52 ± 0.11	0.83	3.26 ± 0.10	0.10	0.21
LVID;s (mm)	2.64 ± 0.12	2.25 ± 0.13	0.08	1.85 ± 0.12	**0.0006**	0.08
FS (%)	27 ± 1	37 ± 2	**0.005**	44 ± 2	**<0.0001**	0.07
LV volume;d (μL)	55 ± 4	53 ± 4	0.85	44 ± 3	0.10	0.20
LV volume;s (μL)	27 ± 3	19 ± 2	0.07	11 ± 2	**0.0005**	0.08
LV mass (mg)	190 ± 8	198 ± 9	0.80	165 ± 11	0.24	**0.05**
heart rate (bpm)	589 ± 17	557 ± 13	0.34	540 ± 20	0.13	0.74

N, number of mice; transstenotic pressure gradient; LVAW, left ventricular anterior wall thickness; d, diastolic; LVPW, left ventricular posterior wall thickness; LVID, left ventricular internal dimension; s, systolic; FS, fractional shortening; bpm, beats per min; mean ± SEM; *P*-values were determined by one-way-ANOVA, values in bold indicate statistically significant results.

Table S5), thereby controlling for these possible flaws. These results further indicated that the observed functional differences between TgPLN and TgAFA-PLN must be caused by the distinct phosphorylation patterns. PKA inhibition by H-89 induced significant changes of baseline inhibitory activity only in TgAFA-PLN (see Supplementary material online, *Figure S7*). Without H-89, monomer phosphorylation of TgAFA-PLN was more than three times stronger compared to TgPLN (*Figure 2*). This result was confirmed by two separate techniques using different antibodies and two further independent transgenic mouse lines (see Supplementary material *online*, *Figure S2A–D*). While TgAFA-PLN seemed to inhibit SERCA2a about as much as TgPLN if PLN was unphosphorylated (see Supplementary material online, *Table S5*), basal PKA activity would be sufficient to almost fully inactivate TgAFA-PLN so that the speed of LV relaxation and contraction is not significantly different from PLN-KO hearts (*Figure 6*, Supplementary material online, *Table S6*).

In the absence of phosphatases or interaction partners other than PKA, we identified higher specificity of PKA for PLN pentamers than for monomers. Subsequent substrate competition between monomers and pentamers resulted in reduced PKA-dependent phosphorylation of monomers. Importantly, we show that pentameric PLN constitutes a direct PKA substrate independent of PLN monomer phosphorylation. S16 phosphorylation by PKA follows a random mechanism, whereas Calmodulin-dependent kinase II (CaMKII) is known to phosphorylate PLN pentamers at T17 via a cooperative mechanism in which phosphorylation of one subunit within a pentamer promotes the phosphorylation of all other protomers within this pentamer.[37,38] In consequence, PLN pentamer phosphorylation increases faster than monomer phosphorylation (see Supplementary material online, *Figure S13*) and—in contrast to Ser16 phosphorylation by PKA—yields two distinct pools of PLN pentamers, i.e. either fully phosphorylated or fully unphosphorylated PLN.[38] Importantly, monomer phosphorylation at T17 was the same in the presence or absence of PLN pentamers, indicating that there is no competition between monomers and pentamers for CaMKII (*Figure 2B*). The unchanged T17 phosphorylation of PLN monomers strongly suggests that the observed functional differences between TgPLN and TgAFA-PLN mostly result from the differences in PLN-S16 phosphorylation. The otherwise unchanged expression and phosphorylation of critical Ca^{2+}-regulatory proteins between TgPLN and TgAFA-PLN hearts as well as the absence of altered Ca^{2+} cycling in the presence of the PKA inhibitor H-89 strongly indicate that reduced S16 phosphorylation of PLN monomers was the decisive cause for delayed Ca^{2+} elimination and myocardial relaxation in the presence of pentamers (see Supplementary material online, *Figure S7 and S8*, Supplementary material online, *Table S5*). However, we cannot exclude that binding of other interaction partners such as 14-3-3 proteins, the direct SERCA activator dwarf open reading frame or S100A1, to a lesser extent contributes to the phosphorylation patterns observed in heart tissue.[39,40]

SERCA2a activity is directly correlated with cardiac contractile performance, and reduced SERCA2a activity is associated with progression to heart failure.[41] Therefore, restoration of depressed myocyte Ca^{2+} transients by either overexpression of SERCA2a or inhibition of PLN has been evaluated as a therapeutic option in the past.[42] Animal models of heart failure demonstrated phenotypic improvement after gene transfer of a dominant-negative PLN mutant,[43] PLN antisense RNAs,[44] intracellular inhibitory PLN antibodies,[45] as well as PLN antisense gene transfer[46] or RNAi targeting of PLN.[47,48] Furthermore, reduced SERCA2a inhibition by increasing PLN phosphorylation via inhibition of protein phosphatase-1 accelerated SR Ca^{2+} uptake and enhanced mechanical recovery after ischaemia/reperfusion injury.[49]

As an alternative to SERCA2a disinhibition, SR Ca^{2+} uptake was accelerated by gene transfer of SERCA2a via adeno-associated virus (AAV1/SERCA2a). This approach improved cardiac haemodynamics and increased survival in experimental models of heart failure.[41,42] Importantly, intracoronary SERCA2a gene delivery to patients with advanced heart failure also demonstrated beneficial effects in a pilot study at 12 months follow-up.[50,51] However, no improved clinical outcome was observed in a larger clinical trial that randomly assigned 250 patients to receive either AAV1/SERCA2a or placebo, possibly due to insufficient expression of SERCA2a by the gene therapy vector.[52] All these strategies against heart failure via enhanced SR Ca^{2+} uptake improved cardiac performance, but it is to date unclear whether they ensure a lasting prevention or regression of heart failure symptoms.

Our studies of TgPLN and TgAFA-PLN mice after TAC propose PLN pentamerization as a critical component for cardiac adaptation to chronic pressure overload (*Figure 7*, *Table 1*). Since SERCA2a is a main ATP consumer of the heart, it is therefore tempting to speculate that unrestrained high SERCA2a activity would cause energetic deficits in the myocardium, at least if further stressors increase myocardial energy demand. Pentamerization extended the dynamic range of SERCA2a activity regulation by increasing the sensitivity of the heart to adrenergic stimulation and allowing the reversion to an energy-saving mode during resting phases (*Figure 6*). If the abilities to regulate the rates of SR Ca^{2+} transport and cardiac relaxation were poor, as in myocardium lacking PLN or expressing purely monomeric PLN, hearts were at risk for dilation and failure despite fast Ca^{2+} kinetics.

Since PLN pentamers add to the regulation of SERCA2a activity, conditions that alter the PLN pentamer-to-monomer ratio would impact on cardiac function. Indeed, various clinical conditions with abnormal pentamer-to-monomer ratios and/or structural alterations of PLN pentamers have been described, which were associated with myocardial

remodelling and functional decline. Examples are carriers of heterozygous PLN mutations, such as the R14del or the R9C mutation, both of which cause lethal, hereditary cardiomyopathy.[16,53] Functionally, the heterozygous mutations result in pentamers with different PKA binding characteristics and impact on the phosphorylation status of SERCA2a-inhibitory monomers as has been demonstrated for the PLN-R9C mutant.[16,22] As such, abnormal pentamerization may contribute to the phenotype caused by these mutations and thereby impact on the development and progression of the disease. It has been shown that the R9C mutation stabilizes the PLN pentameric assembly, particularly under conditions of oxidative stress, thereby possibly modulating the cardiotoxic effects of the mutation.[54]

Furthermore, the pentamer-to-monomer ratio is strongly dependent on total PLN concentrations and thus may be altered under conditions of decreased PLN expression[15] (see Supplementary material online, *Figure S14*). Apart from loss-of-function mutations, decreased expression of healthy PLN has been described in pathological conditions including experimental models of late-stage heart failure after myocardial infarction, hyperthyroidism, as well as aging hearts.[55–57] Also, pharmacons may reduce PLN expression as the administration of acetylsalicylic acid was found to be negatively correlated with the expression of PLN in human right atrial biopsies.[58] Finally, it has been shown that the presence of SERCA2a promotes depolymerization of PLN pentamers,[59] suggesting that all conditions of SERCA2a up- or down-regulation would modulate the degree of PLN pentamerization. Taken together, the PLN pentamer-to-monomer ratio can be altered under multiple physiological and pathophysiological conditions. The latter are often associated with myocardial dysfunction, and targeted intervention in the amount or ratio of PLN pentamers and monomers may lead to therapeutic opportunities.

Supplementary material

Supplementary material is available at *Cardiovascular Research* online.

Author contributions

F.F. designed, performed and analysed experiments and edited the manuscript; A.K., K.H., and M.B. performed experiments and quantification; M.O. and G.K. provided vital reagents, D.K. provided intellectual input and discussion; J.P.S. conceived and supervised the study, performed and analysed the *in vivo* experiments and wrote the manuscript. All authors proofread the manuscript.

Acknowledgements

We thank B. Thur, M. Babl and S. Hölzer for excellent technical assistance.

Conflict of interests: None declared.

Funding

This work was supported by the Deutsche Forschungsgemeinschaft (DFG, German Research Foundation) [236177352- SFB 1116, TPA02 to J.P.S.] and [SCHM1493/4-1 to J.P.S].

Data availability

The data underlying this article are available in the article and in its online supplementary material.

References

1. Bers DM. Calcium fluxes involved in control of cardiac myocyte contraction. *Circ Res* 2000; **87**:275–281.
2. Mattiazzi A, Mundiña-Weilenmann C, Guoxiang C, Vittone L, Kranias E. Role of phospholamban phosphorylation on Thr17 in cardiac physiological and pathological conditions. *Cardiovasc Res* 2005;**68**:366–375.
3. Cornea RL, Jones LR, Autry JM, Thomas DD. Mutation and phosphorylation change the oligomeric structure of phospholamban in lipid bilayers. *Biochemistry* 1997;**36**:2960–2967.
4. Simmerman HKB, Kobayashi YM, Autry JM, Jones LR. A leucine zipper stabilizes the pentameric membrane domain of phospholamban and forms a coiled-coil pore structure. *J Biol Chem* 1996;**271**:5941–5946.
5. Kimura Y, Kurzydlowski K, Tada M, MacLennan DH. Phospholamban inhibitory function is activated by depolymerization. *J Biol Chem* 1997;**272**:15061–15064.
6. Zvaritch E, Backx PH, Jirik F, Kimura Y, De Leon S, Schmidt AG, Hoit BD, Lester JW, Kranias EG, MacLennan DH. The transgenic expression of highly inhibitory monomeric forms of phospholamban in mouse heart impairs cardiac contractility. *J Biol Chem* 2000;**275**: 14985–14991.
7. Autry JM, Jones LR. Functional co-expression of the canine cardiac Ca^{2+}pump and phospholamban in spodoptera frugiperda (Sf21) cells reveals new insights on ATPase regulation. *J Biol Chem* 1997;**272**:15872–15880.
8. MacLennan DH, Toyofuku T, Kimura Y. Sites of regulatory interaction between calcium ATPases and phospholamban. *Basic ResCardiol* 1997;**92**:11–15.
9. Hou Z, Kelly EM, Robia SL. Phosphomimetic mutations increase phospholamban oligomerization and alter the structure of its regulatory complex. *J Biol Chem* 2008;**283**: 28996–29003.
10. Glaves JP, Trieber CA, Ceholski DK, Stokes DL, Young HS. Phosphorylation and mutation of phospholamban alter physical interactions with the sarcoplasmic reticulum calcium pump. *J Mol Biol* 2011;**405**:707–723.
11. Stokes DL, Pomfret AJ, Rice WJ, Glaves JP, Young HS. Interactions between Ca^{2+}-ATPase and the pentameric form of phospholamban in two-dimensional co-crystals. *Biophys J* 2006;**90**:4213–4223.
12. Glaves JP, Primeau JO, Espinoza-Fonseca LM, Lemieux MJ, Young HS. The phospholamban pentamer alters function of the sarcoplasmic Reticulum calcium pump SERCA. *Biophys J* 2019;**116**:633–647.
13. Ceholski DK, Trieber CA, Holmes CFB, Young HS. Lethal, hereditary mutants of phospholamban elude phosphorylation by protein kinase A. *J Biol Chem* 2012;**287**:26596–26605.
14. Wittmann T, Lohse MJ, Schmitt JP. Phospholamban pentamers attenuate PKA-dependent phosphorylation of monomers. *J Mol Cell Cardiol* 2015;**80**:90–97.
15. Koch D, Alexandrovich A, Funk F, Kho AL, Schmitt JP, Gautel M. Molecular noise filtering in the β-adrenergic signaling network by phospholamban pentamers. *Cell Rep* 2021;**36**:109448.
16. Schmitt JP, Kamisago M, Asahi M, Li GH, Ahmad F, Mende U, Kranias EG, MacLennan DH, Seidman JG, Seidman CE. Dilated cardiomyopathy and heart failure caused by a mutation in phospholamban. *Science* 2003;**299**:1410–1413.
17. Schmid E, Neef S, Berlin C, Tomasovic A, Kahlert K, Nordbeck P, Deiss K, Denzinger S, Herrmann S, Wettwer E, Weidendorfer M, Becker D, Schäfer F, Wagner N, Ergün S, Schmitt JP, Katus HA, Weidemann F, Ravens U, Maack C, Hein L, Ertl G, Müller OJ, Maier LS, Lohse MJ, Lorenz K. Cardiac RKIP induces a beneficial β-adrenoceptor–dependent positive inotropy. *Nat Med* 2015;**21**:1298–1306.
18. Haghighi K, Pritchard T, Bossuyt J, Waggoner JR, Yuan Q, Fan GC, Osinska H, Anjak A, Rubinstein J, Robbins J, Bers DM, Kranias EG. The human phospholamban Arg14-deletion mutant localizes to plasma membrane and interacts with the Na/K-ATPase. *J Mol Cell Cardiol* 2012;**52**:773–782.
19. Schmitt JP, Semsarian C, Arad M, Gannon J, Ahmad F, Duffy C, Lee RT, Seidman CE, Seidman JG. Consequences of pressure overload on sarcomere protein mutation-induced hypertrophic cardiomyopathy. *Circulation* 2003;**108**:1133–1138.
20. Lorenz K, Schmitt JP, Schmitteckert EM, Lohse MJ. A new type of ERK1/2 autophosphorylation causes cardiac hypertrophy. *Nat Med* 2008;**15**:75–83.
21. Blankenburg R, Hackert K, Wurster S, Deenen R, Seidman JG, Seidman CE, Lohse MJ, Schmitt JP. β-Myosin heavy chain variant Val606Met causes very mild hypertrophic cardiomyopathy in mice, but exacerbates HCM phenotypes in mice carrying other HCM mutations. *Circ Res* 2014;**115**:227–237.
22. Schmitt JP, Ahmad F, Lorenz K, Hein L, Schulz S, Asahi M, Maclennan DH, Seidman CE, Seidman JG, Lohse MJ. Alterations of phospholamban function can exhibit cardiotoxic effects independent of excessive sarcoplasmic reticulum Ca^{2+}-ATPase inhibition. *Circulation* 2009;**119**:436–444.
23. Wu Y, Li Q, Chen XZ. Detecting protein–protein interactions by far western blotting. *Nat Protoc* 2007;**2**:3278–3284.
24. Livak KJ, Schmittgen TD. Analysis of relative gene expression data using real-time quantitative PCR and the 2(-Delta Delta C(T)) method. *Methods* 2001;**25**:402–408.
25. Robia SL, Campbell KS, Kelly EM, Hou Z, Winters DL, Thomas DD. Förster transfer recovery reveals that phospholamban exchanges slowly from pentamers but rapidly from the SERCA regulatory complex. *Circ Res* 2007;**101**:1123–1129.
26. Karim CB, Marquardt CG, Stamm JD, Barany G, Thomas DD. Synthetic null-cysteine phospholamban analogue and the corresponding transmembrane domain inhibit the Ca-ATPase. *Biochemistry* 2000;**39**:10892–10897.
27. Verardi R, Shi L, Traaseth NJ, Walsh N, Veglia G. Structural topology of phospholamban pentamer in lipid bilayers by a hybrid solution and solid-state NMR method. *Proc Natl Acad Sci* 2011;**108**:9101–9106.
28. Gustavsson M, Verardi R, Mullen DG, Mote KR, Traaseth NJ, Gopinath T, Veglia G. Allosteric regulation of SERCA by phosphorylation-mediated conformational shift of phospholamban. *Proc Natl Acad Sci* 2013;**110**:17338–17343.
29. MacLennan DH, Kranias EG. Phospholamban: a crucial regulator of cardiac contractility. *Nat Rev Mol Cell Biol* 2003;**4**:566–577.
30. Schellenberger V, Siegel RA, Rutter WJ. Analysis of enzyme specificity by multiple substrate kinetics. *Biochemistry* 2002;**32**:4344–4348.

31. Anderson VE. Multiple alternative substrate kinetics. *Biochim Biophys Acta* 2015;**1854**: 1729–1736.
32. Luo W, Grupp IL, Harrer J, Ponniah S, Grupp G, Duffy JJ, Doetschman T, Kranias EG. Targeted ablation of the phospholamban gene is associated with markedly enhanced myocardial contractility and loss of beta-agonist stimulation. *Circ Res* 1994;**75**:401–409.
33. Akin BL, Hurley TD, Chen Z, Jones LR. The structural basis for phospholamban inhibition of the calcium pump in sarcoplasmic reticulum. *J Biol Chem* 2013;**288**:30181–30191.
34. Asahi M, Kurzydlowski K, Tada M, MacLennan DH. Sarcolipin inhibits polymerization of phospholamban to induce superinhibition of sarco(endo)plasmic reticulum Ca^{2+}-ATPases (SERCAs). *J Biol Chem* 2002;**277**:26725–26728.
35. Chu G, Li L, Sato Y, Harrer JM, Kadambi VJ, Hoit BD, Bers DM, Kranias EG. Pentameric assembly of phospholamban facilitates inhibition of cardiac function in vivo. *J Biol Chem* 1998; **273**:33674–33680.
36. Menzel J, Kownatzki-Danger D, Tokar S, Ballone A, Unthan-Fechner K, Kilisch M, Lenz C, Urlaub H, Mori M, Ottmann C, Shattock MJ, Lehnart SE, Schwappach B. 14-3-3 Binding creates a memory of kinase action by stabilizing the modified state of phospholamban. *Sci Signal* 2020;**13**:eaaz1436.
37. Li C, Wang JH, Colyer J. Immunological detection of phospholamban phosphorylation states facilitates the description of the mechanism of phosphorylation and dephosphorylation. *Biochemistry* 1990;**29**:4535–4540.
38. Jackson WA, Colyer J. Translation of Ser16 and Thr17 phosphorylation of phospholamban into Ca^{2+}-pump stimulation. *Biochem J* 1996;**316**:201–207.
39. Fisher ME, Bovo E, Aguayo-Ortiz R, Cho EE, Pribadi MP, Dalton MP, Rathod N, Lemieux MJ, Espinoza-Fonseca LM, Robia SL, Zima AV, Young HS. Dwarf open reading frame (DWORF) is a direct activator of the sarcoplasmic reticulum calcium pump SERCA. *Elife* 2021;**10**: e65545.
40. Kiewitz R, Acklin C, Schäfer BW, Maco B, Uhrík B, Wuytack F, Erne P, Heizmann CW. Ca^{2+}-dependent interaction of S100A1 with the sarcoplasmic reticulum Ca^{2+}-ATPase2a and phospholamban in the human heart. *Biochem Biophys Res Commun* 2003;**306**:550–557.
41. Eisner D, Caldwell J, Trafford A. Sarcoplasmic reticulum Ca-ATPase and heart failure 20 years later. *Circ Res* 2013;**113**:958–961.
42. Kho C, Lee A, Hajjar RJ. Altered sarcoplasmic reticulum calcium cycling—targets for heart failure therapy. *Nat Rev Cardiol* 2012;**9**:717–733.
43. Kaye DM, Preovolos A, Marshall T, Byrne M, Hoshijima M, Hajjar R, Mariani JA, Pepe S, Chien KR, Power JM. Percutaneous cardiac recirculation-mediated gene transfer of an inhibitory phospholamban peptide reverses advanced heart failure in large animals. *J Am Coll Cardiol* 2007;**50**:253–260.
44. Tsuji T, Del MF, Yoshikawa Y, Abe T, Shimizu J, Nakajima-Takenaka C, Taniguchi S, Hajjar RJ, Takaki M. Rescue of Ca^{2+}overload-induced left ventricular dysfunction by targeted ablation of phospholamban. *Am J Physiol Hear Circ Physiol* 2009;**296**:310–317.
45. Dieterle T, Meyer M, Gu Y, Belke DD, Swanson E, Iwatate M, Hollander J, Peterson KL, Ross J, Dillmann WH. Gene transfer of a phospholamban-targeted antibody improves calcium handling and cardiac function in heart failure. *Cardiovasc Res* 2005;**67**:678–688.
46. Del Monte F, Harding SE, Dec GW, Gwathmey JK, Hajjar RJ. Targeting phospholamban by gene transfer in human heart failure. *Circulation* 2002;**105**:904–907.
47. Suckau L, Fechner H, Chemaly E, Krohn S, Hadri L, Kockskamper J, Westermann D, Bisping E, Ly H, Wang X, Kawase Y, Chen J, Liang L, Sipo I, Vetter R, Weger S, Kurreck J, Erdmann V, Tschope C, Pieske B, Lebeche D, Schultheiss HP, Hajjar RJ, Poller WC. Long-term cardiac-targeted RNA interference for the treatment of heart failure restores cardiac function and reduces pathological hypertrophy. *Circulation* 2009;**119**:1241–1252.
48. Beverborg NG, Später D, Knöll R, Hidalgo A, Yeh ST, Elbeck Z, Silljé HHW, Eijgenraam TR, Siga H, Zurek M, Palmér M, Pehrsson S, Albery T, Bomer N, Hoes MF, Boogerd CJ, Frisk M, van Rooij E, Damle S, Louch WE, Wang QD, Fritsche-Danielson R, Chien KR, Hansson KM, Mullick AE, de Boer RA, van der Meer P. Phospholamban antisense oligonucleotides improve cardiac function in murine cardiomyopathy. *Nat Commun* 2021;**12**:1–15.
49. Nicolaou P, Rodriguez P, Ren X, Zhou X, Qian J, Sadayappan S, Mitton B, Pathak A, Robbins J, Hajjar RJ, Jones K, Kranias EG. Inducible expression of active protein phosphatase-1 inhibitor-1 enhances basal cardiac function and protects against ischemia/reperfusion injury. *Circ Res* 2009;**104**:1012–1020.
50. Jessup M, Greenberg B, Mancini D, Cappola T, Pauly DF, Jaski B, Yaroshinsky A, Zsebo KM, Dittrich H, Hajjar RJ. Calcium upregulation by percutaneous administration of gene therapy in cardiac disease (CUPID): a phase 2 trial of intracoronary gene therapy of sarcoplasmic reticulum Ca^{2+}-ATPase in patients with advanced heart failure. *Circulation* 2011;**124**: 304–313.
51. Zsebo K, Yaroshinsky A, Rudy JJ, Wagner K, Greenberg B, Jessup M, Hajjar RJ. Long-term effects of AAV1/SERCA2a gene transfer in patients with severe heart failure: analysis of recurrent cardiovascular events and mortality. *Circ Res* 2014;**114**:101–108.
52. Greenberg B, Butler J, Felker GM, Ponikowski P, Voors AA, Desai AS, Barnard D, Bouchard A, Jaski B, Lyon AR, Pogoda JM, Rudy JJ, Zsebo KM. Calcium upregulation by percutaneous administration of gene therapy in patients with cardiac disease (CUPID 2): a randomised, multinational, double-blind, placebo-controlled, phase 2b trial. *Lancet* 2016;**387**:1178–1186.
53. Haghighi K, Kolokathis F, Gramolini AO, Waggoner JR, Pater L, Lynch RA, Fan GC, Tsiapras D, Parekh RR, Dorn GW, MacLennan DH, Kremastinos DT, Kranias EG. A mutation in the human phospholamban gene, deleting arginine 14, results in lethal, hereditary cardiomyopathy. *Proc Natl Acad Sci U S A* 2006;**103**:1388–1393.
54. Ha KN, Mastersona LR, Hou Z, Verardi R, Walsh N, Veglia G, Robia SL. Lethal Arg9Cys phospholamban mutation hinders Ca^{2+}-ATPase regulation and phosphorylation by protein kinase A. *Proc Natl Acad Sci U S A* 2011;**108**:2735–2740.
55. Mørk HK, Sjaastad I, Sande JB, Periasamy M, Sejersted OM, Louch WE. Increased cardiomyocyte function and Ca^{2+}transients in mice during early congestive heart failure. *J Mol Cell Cardiol* 2007;**43**:177–186.
56. Kiss E, Ball NA, Kranias EG, Walsh RA. Differential changes in cardiac phospholamban and sarcoplasmic reticular Ca^{2+}-ATPase protein levels. *Circ Res* 1995;**77**:759–764.
57. Jiang MT, Moffat MP, Narayanan N. Age-related alterations in the phosphorylation of sarcoplasmic reticulum and myofibrillar proteins and diminished contractile response to isoproterenol in intact rat ventricle. *Circ Res* 1993;**72**:102–111.
58. Gergs U, Mangold W, Langguth F, Hatzfeld M, Hauptmann S, Bushnaq H, Simm A, Silber RE, Neumann J. Alterations of protein expression of phospholamban, ZASP and plakoglobin in human atria in subgroups of seniors. *Sci Rep* 2019;**9**:1–10.
59. Reddy LG, Jones LR, Thomas DD. Depolymerization of phospholamban in the presence of calcium pump: a fluorescence energy transfer study. *Biochemistry* 1999;**38**:3954–3962.

Translational perspective

Pentamerization of phospholamban (PLN) adds to the regulation of cardiac contractile function and facilitates myocardial transition to an energy-saving mode during resting phases. Thus, PLN pentamers would protect cardiomyocytes from energetic deficits, and they improve stress adaptation of the heart as shown for sustained pressure overload in this study. Strategies that target PLN pentamerization promise therapeutic potential in the treatment of myocardial maladaptation to stress as well as cardiac pathologies associated with altered monomer-to-pentamer ratios, e.g. cardiomyopathies due to PLN mutations, certain types of heart failure, and aged hearts.